Redox Properties of the [2Fe-2S] Center in the 24 kDa (NQO2) Subunit of NADH:Ubiquinone Oxidoreductase (Complex I)†

Yanbing Zu,‡,§ Salvatore Di Bernardo,‡,|| Takao Yagi,|| and Judy Hirst*,§

Medical Research Council Dunn Human Nutrition Unit, Wellcome Trust/MRC Building, Hills Road, Cambridge CB2 2XY, U.K., and Division of Biochemistry, Department of Molecular and Experimental Medicine, The Scripps Research Institute, La Jolla, California 92037

Received April 25, 2002; Revised Manuscript Received June 10, 2002

ABSTRACT: The redox properties of the [2Fe-2S] cluster in the 24 kDa subunit of bovine heart mitochondrial NADH:ubiquinone oxidoreductase (complex I) and three of its homologues have been defined using protein−film voltammetry. The clusters in all four examples display characteristic, pH-dependent redox transitions, which, unusually, can be masked by high ionic strength conditions. At low ionic strength (10 mM NaCl) the reduction potential varies by approximately 100 mV between high and low pH limits (pH 5 and 9); thus the redox process is not strongly coupled and is unlikely to form part of the mechanism of energy transduction in complex I. The pH dependence was shown to result from pH-linked changes in protein charge, due to nonspecific protonation events, rather than from the coupling of a specific ionizable residue, and the ionic strength dependence at high and low pH was modeled using extended Debye−Hückel theory. The low potential of the 24 kDa subunit [2Fe-2S] cluster, out of line with the potentials of the other iron−sulfur clusters in complex I, is suggested to play a role in coupling reducing equivalents at the catalytic active site. Finally, the validity of using the [2Fe-2S] cluster in an isolated subunit, as a mechanistic basis for coupled proton−electron transfer in intact complex I, is evaluated.

Mitochondrial NADH:ubiquinone oxidoreductase (complex I)[1] is the entry point for electrons into the membrane-bound respiratory chain (*1*, *2*). Complex I catalyzes the two-electron oxidation of NADH to NAD^+ and the concomitant reduction of ubiquinone to ubiquinol, a process which is coupled to proton translocation across the inner mitochondrial membrane (*3*, *4*). At present, complex I is the least understood of the three proton-pumping complexes which create the proton-motive force across the inner mitochondrial membrane, used for ATP production. Structural information on the L-shaped assembly is limited to 22 Å resolution (*5*), and little is known about how the energy liberated by the electron transfer process is coupled to vectorial proton translocation.

Complex I from bovine heart mitochondria consists of at least 43 different subunits, the primary structures of which have been determined (*3*, *6*, *7*). Bacterial NADH:quinone oxidoreductases (*8*, *9*), which have fewer subunits (13 or 14), contain homologues to all the proposed cofactor binding subunits of the mitochondrial enzyme, indicating a similar fundamental mechanism for electron transfer. Complex I is now thought likely to contain two [2Fe-2S] clusters and six [4Fe-4S] clusters (*10*−*12*); on the basis of primary sequence analysis (*3*) and the overexpression of individual, cofactor-containing subunits (*13*−*17*), information about the subunit location and properties of each cluster is now being consolidated, though ambiguities still remain. Mechanistically, it is a reasonable assumption that electrons enter complex I at the noncovalently bound flavin mononucleotide (FMN) active site, where NADH is oxidized, and are then passed along by the Fe−S clusters to one or more spatially removed quinone-binding site(s), where Q is reduced to QH_2. The point at which the available energy is "siphoned off" for vectorial proton transfer is not known. One possibility is a coupled electron−proton transfer event at one (or more) of the redox sites; consequently, the pH dependence of an iron−sulfur reduction potential would be a key indicator of this type of event (*18*, *19*).

The 24 kDa subunit of mitochondrial complex I (*20*) is homologous to the NQO2 subunit of *Paracoccus denitrificans* (*21*) and *Thermus thermophilus* (*22*) and the NUOE subunit of *Escherichia coli* (*23*). For simplicity, the term "24 kDa subunit" is used generically, throughout this paper, to refer to the mitochondrial protein and also its homologues. The 24 kDa subunit is one of the better characterized subunits of complex I, and there can be little doubt that it houses a [2Fe-2S] cluster. A [2Fe-2S] binding motif (*24*, *25*), Cys-$(X)_4$-Cys-$(X)_{35}$-Cys-$(X)_3$-Cys, is conserved through all known complex I 24 kDa subunits and, while less common than

† This work was supported by the Medical Research Council, by U.S. Public Health Service Grants R01GM33712 and M01RR00833, and by the Sam and Rose Stein Endowment Fund.

* To whom correspondence should be addressed. Tel: +44 1223 252810. Fax: +44 1223 252815. E-mail: jh@mrc-dunn.cam.ac.uk.

‡ These authors contributed equally to this work.

§ Medical Research Council Dunn Human Nutrition Unit.

|| The Scripps Research Institute.

[1] Abbreviations: complex I, NADH:(ubi)quinone oxidoreductase; DTT, dithiothreitol; EPR, electron paramagnetic resonance; Fe-S, iron−sulfur cluster; FMN, flavin mononucleotide; Fp, flavoprotein fragment of complex I; *I*, ionic strength; NADH, *β*-nicotinamide adenine dinucleotide (reduced form); PMSF, phenylmethanesulfonyl fluoride; Q and QH_2, quinone and quinol; 24 kDa protein, NQO2, NUOE, subunit of complex I.

10.1021/bi026026f CCC: $22.00
Published on Web 07/13/2002

the plant-type or hydroxylase-type 2Fe−ferredoxin motifs [Cys-$(X)_4$-Cys-$(X)_2$-Cys-$(X)_{29}$-Cys and Cys-$(X)_5$-Cys-$(X)_2$-Cys-$(X)_{36/37}$-Cys (*26*)], also occurs in a number of hydrogenases typified by the NADP-reducing hydrogenase from *Desulfovibrio fructosovorans* (*27*) and the complex iron-only hydrogenase from *Thermotoga maritima* (*28*). A similar motif, Cys-$(X)_{12}$-Cys-$(X)_{31/32}$-Cys-$(X)_3$-Cys, is also observed in the [2Fe-2S] ferredoxins from *Clostridium pasteurianum*, *Azotobacter vinelandii* (*29*), and *Aquifex aeolicus*; the latter has recently been shown to have a thioredoxin-like fold, with the [2Fe-2S] cluster located close to the solvent-accessible surface (*25*, *30*). The spectroscopic properties of the [2Fe-2S] cluster in the 24 kDa subunit, as typified by the overexpressed *P. denitrificans* homologue, also place this complex I cluster firmly in the *C. pasteurianum* subclass of [2Fe-2S] ferredoxins, spectroscopically distinct from those of plant or hydroxylase type (*31*). Furthermore, "swapping" the second cysteine ligand of *C. pasteurianum* ferredoxin into a position analogous to that taken in the complex I 24 kDa subunits [Cys-$(X)_4$-Cys-$(X)_{39}$-Cys-$(X)_3$-Cys] produced a protein which retained the spectroscopic properties of the native cluster (*32*). Taken together, these observations strongly suggest a common fold for the complex I 24 kDa subunits and within the *C. pasteurianum* subclass of [2Fe-2S] ferredoxins (*25*).

Within intact complex I, the 24 kDa subunit is almost certainly located adjacent to the 51 kDa subunit, which houses the FMN active site at which NADH is bound and oxidized (*3*). The 51 kDa subunit is also thought to contain a [4Fe-4S] cluster (*3*, *10*, *11*, *14*), and either this cluster or the 24 kDa [2Fe-2S] cluster is likely to be the initial acceptor of electrons from the active site. Since iron−sulfur clusters are one-electron carriers, but the oxidation of NADH is a two-electron process, the initial cluster may have an important influence on the lifetime of intermediate, radical states at the active site. Direct evidence for the close association of the 51 and 24 kDa subunits in complex I has been provided by fractionation of the bovine mitochondrial enzyme by the chaotrophic ion perchlorate, producing the catalytically active and soluble "Fp" subcomplex, consisting of only the 51, 24, and 10 kDa subunits (*33*). *E. coli* complex I has also been fractionated to produce a fragment consisting of the NuoE, NuoF, and NuoG (24, 51, and 75 kDa) subunits (*34*). In addition, while all attempts to overexpress an active form of the isolated 51 kDa subunit have so far failed, coexpression of the 51 and 24 kDa subunits produced an "Fp-type" enzyme which displayed some NADH-oxidizing ability (*14*). Finally, the soluble NAD-reducing hydrogenase from *Ralstonia eutropha* (formerly *Alcaligenes eutrophus*) contains four subunits, two of which form an FMN-containing NADH oxidoreductase dimer. Of these two subunits, one is a fusion of homologues to the 24 and 51 kDa subunits of complex I, while the second is homologous to part of the 75 kDa subunit, again strongly suggesting that the 51 and 24 kDa subunits constitute a structural unit within complex I (*35*).

To date, electron paramagnetic resonance (EPR) has been the predominant technique for studying the redox properties of the iron−sulfur clusters in complex I (*10*, *11*), since iron−sulfur clusters, unlike heme groups, for example, lack distinctive optical spectral features. However, studies of individual centers have been hampered by difficulties in resolving the numerous overlapping signals and by possible complications arising from spin−spin interactions, low and therefore inaccessible redox potentials, and $S > {}^1/_2$ ground states. In addition, EPR redox titrations, carried out over a range of pH values, are expensive in both time and amount of protein required. We now describe the application of protein−film voltammetry (*36*, *37*) to the study of the redox mechanism of complex I. Protein−film voltammetry allows the measurement, deconvolution, and quantification of both the kinetics and thermodynamics of complex, coupled electron transfer reactions in a single set of experiments (*18*, *19*, *38*−*41*). In this publication we address the redox properties of the [2Fe-2S] cluster in the overexpressed complex I 24 kDa subunit of four distinct homologues. Mechanistically, the 24 kDa subunit cluster is particularly interesting because of its location close to the active site and since EPR studies have reported its reduction potential to be pH-dependent (*10*, *11*). The accuracy and reproducibility of our measurements, using comparatively minute amounts of sample, have allowed investigation of a wide range of pH, ionic strength, and temperature and have consequently enabled the first comprehensive description of the redox properties of this important cluster. In addition, the simplification which results from studying, in isolation, a single component of this complex machine provides valuable spectroscopic and redox information to complement studies of the intact enzyme. Finally, the implications of our results for the mechanism of complex I are discussed.

EXPERIMENTAL PROCEDURES

Cloning, Overexpression, and Site-Directed Mutagenesis. The genes encoding the 24 kDa subunits from bovine heart mitochondria (*20*) and *E. coli* (*23*) were cloned into the expression plasmid pMW172 (*42*). DNA was amplified by PCR from bovine heart cDNA and *E. coli* DNA, respectively, using expand DNA polymerase (Roche Diagnostics Gmbh) and the following primers: bovine forward primer, TAGGAATTCCATATGGGAGCTGGAGGAGCCTTATTTG; bovine reverse primer, CGAAAGCTTTTAAAGGCCTGCTTGCACACC; *E. coli* forward primer, TAGGAATTCCATATGCACGAGAATCAACAACCAC; *E. coli* reverse primer, CGAAAGCTTTCATTTATACCGCTCCAGCAGTTCAGGG. Following digestion with the appropriate restriction enzymes, *Nde*I and *Hin*dIII (New England Biolabs Inc.; restriction sites underlined), the insert was ligated into the expression vector and checked by direct sequencing. When required, an N-terminal histidine tag was added by incorporating 7 (*E. coli* homologue) or 10 (bovine homologue) histidine codons into the 5′-primer sequence. Ca^{2+}-competent *E. coli* cells, strain C41(DE3) (*43*), were transformed and grown overnight, at 37 °C, on a TYE-agar plate containing 100 μg mL^{-1} ampicillin, and single colonies were then used to inoculate 4 × 1 L of 2 × TY medium (16 g L^{-1} tryptone, 10 g L^{-1} yeast extract, 5 g L^{-1} NaCl, pH 7.4) containing 100 μg mL^{-1} ampicillin (Melford Laboratories Ltd.) and supplemented with 10 μM cysteine and 10 μM ferric ammonium citrate (Sigma-Aldrich Ltd.). Cells were grown aerobically at 37 °C to an optical density of 0.6 at 600 nm, when protein overexpression was induced by the addition of isopropyl β-D-thiogalactopyranoside (IPTG; Melford Laboratories Ltd.) to a final concentration of 0.6 mM. Following overnight growth at 25 °C the cells were harvested

by centrifugation, resuspended in 50 mM Tris-HCl (pH 8), containing 2 mM dithiothreitol (DTT) and 0.001% (w/v) phenylmethanesulfonyl fluoride (PMSF), and frozen at −20 °C for storage.

The genes encoding the *P. denitrificans* and *T. thermophilus* NQO2 subunits were cloned from the pXT-1 (*44*) and pTTH-1 (*22*) plasmids, respectively. To generate *Nde*I and *Xho*I restriction sites, the sense and antisense primers GACCGC*AT*ATGCTGCGCCGTC and CTGCTC*GAG*TTC-GATTAGACG were used to amplify the *P. denitrificans* gene; italic bases were altered from the genomic DNA. In the same way, for the *T. thermophilus* gene, the sense primer GGGAGGGC*AT*ATGGGGTTCTTTGACG was used to generate an *Nde*I restriction site, and the antisense primers GGAAAG*AAGCTT*GCCAGTCATACC and GAA*AGATCT*-GGGCCAGTCATACC were used to generate *Hin*dIII and *Bgl*II restriction sites, respectively. The DNA fragments generated by PCR amplification were ligated into pCRScript cloning vectors (Stratagene, La Jolla, CA) according to the manufacturer's protocol and checked by direct sequencing. Subsequently, these plasmids were digested with the appropriate restriction endonucleases, and the DNA fragments were cloned into the pET16b and pET24a expression plasmids. pET24a-TthNQO2 was used to overexpress the nonfused, wild-type *T. thermophilus* NQO2 protein, while pET16b-PdNQO2 and pET16b-TthNQO2 produced proteins fused to a 10-residue histidine tag at the N-terminus. The proteins were expressed in *E. coli* strain BL21(DE3)pLysS, as described previously, with the growth medium supplemented by 100 μg L^{-1} ferric ammonium citrate and 100 μM Na_2S (*14*).

Mutagenesis of the *T. thermophilus* NQO2 subunit was carried out on the pCRScript-TthNQO2 plasmid, using a mutagenesis kit (Promega Corp., Madison, WI), according to manufacturer's instructions. The following oligonucleotides were used: (i) H79A, CCCACGGGGAAGTAC*GC*-*C*CTCCAGGTCTGCGCC; (ii) D114N, CCGGGGGAGGT-GACCCCG*A*ACGGGCTTTTCAGCGTG; (iii) E123Q, GC-GTGCAGA*A*GGTG*C*AGTGCCTGGGAAGC; (iv) H129A, GCCTGGGAAGCTGC*GC*CACCGCCCCCGTGA. All mutants were checked by direct sequencing. The TthNQO2 fragments carrying the mutated oligonucleotides were then cloned into the pET16b expression plasmid and overexpressed as described above.

Protein Purification. (i) Bovine Mitochondrial 24 kDa Protein (without Histidine Tag) (45). Cells were thawed on ice and broken by passage through a cell disrupter (Constant Systems Ltd., Kenilworth, U.K.) at 30000 psi; insoluble cell debris was removed by centrifugation (48000*g*, 10 min). DTT (1 mM) was added and maintained throughout, and all steps were carried out at 4 °C. Streptomycin sulfate was added to 1% (w/v) while stirring on ice, and the white precipitate was removed by centrifugation (48000*g*, 20 min). Following dialysis (into 50 mM Tris-HCl at pH 8), the protein solution was pumped through a DE52 anion-exchange column (Whatman International Ltd.), preequilibrated in the same buffer, removing a number of contaminating proteins. The flow-through was then loaded directly onto a Q-Sepharose column (Amersham Pharmacia Biotechnology, AB), again preequilibrated in 50 mM Tris-HCl at pH 8, and eluted with a linear NaCl gradient; the 24 kDa protein eluted at approximately 0.2 M NaCl. Fractions were pooled and concentrated by ammonium sulfate precipitation (35% saturation). The dark red-brown pellet was redissolved into a minimum volume and run on a gel filtration column (Sephacryl S-100, Amersham Pharmacia Biotechnology, AB) in 0.2 M NaCl and 50 mM Tris-HCl, pH 8, buffer. Elution occurred in two peaks, both of high purity as judged by SDS−PAGE analysis, which are considered to consist of dimers and monomers; monomer fractions were collected, pooled, and transferred into an anaerobic glovebox (O_2 < 1 ppm; Belle Technology) before being concentrated to approximately 200 μM using a YM10 membrane (Millipore Corp., Bedford, MA). Although the homologous proteins from *C. pasteurianum* and *A. aeolicus* are dimerized in the native state and in the crystal structure (*30*), maintaining the 24 kDa protein anaerobically greatly reduced conversion of any of this monomeric fraction into the dimeric form, as observed if the protein was stored aerobically; the dimeric form is therefore likely to be mainly the result of oxygen-induced cluster loss and dimerization via the free sulfhydryl groups formed.

(ii) Bovine Mitochondrial and E. coli Histidine-Tagged Homologues. The cytoplasmic cell fraction was obtained by lysis and centrifugation as described above, then filtered before being transferred into an anaerobic glovebox (O_2 < 1 ppm), and purified by Ni-NTA affinity chromatography (Qiagen GmbH). Two column wash steps of 10 and 20 mM imidazole in 50 mM sodium phosphate buffer with 300 mM NaCl, pH 8.0, were employed, and then the proteins were eluted using 250 mM imidazole; purity was confirmed by SDS−PAGE analysis.

(iii) P. denitrificans and T. thermophilus Homologues. Histidine-tagged *P. denitrificans* and *T. thermophilus* 24 kDa subunits were purified according to the method of Yano et al. (*14*) with minor modifications. Briefly, cells were harvested by centrifugation (6000*g*, 10 min) and then resuspended in a deoxygenated 50 mM Tris-HCl buffer (pH 7.4, 1 mM DTT, 300 mM NaCl, 0.1 mM PMSF) at a ratio of 10% w/v. The cell suspension was passed through a French press (25000 psi), and cell debris was removed by centrifugation (23500*g*, 15 min). Following ultracentrifugation (180000*g*, 30 min), the resulting supernatant was collected and transferred immediately into an anaerobic glovebox (COY Laboratory Products Inc.), where all subsequent procedures were performed, limiting oxidative cluster degradation. The histidine-tagged proteins were purified by Ni-NTA affinity chromatography (Qiagen GmbH), and their purity was checked by SDS−PAGE analysis. For the nonfused *T. thermophilus* subunit, a 5 min, 65 °C heat treatment was followed by a 10 min, 32000*g* centrifugation, removing many nonthermostable *E. coli* proteins. The supernatant was then loaded onto an anion-exchange column (DEAE Toyopearl, Tosho Corp.) and eluted by an NaCl step gradient (10 mM Tris-HCl, pH 8.0); the 24 kDa subunit eluted in 100−200 mM NaCl. Finally, the protein was purified to homogeneity (as judged by SDS−PAGE) using a Sephadex G-75 gel filtration column (Amersham Pharmacia Biotech AB; 10 mM Tris-HCl, 150 mM NaCl, pH 8.0) and concentrated in a YM10 Centriprep concentrator (Millipore Corp., Bedford, MA). *T. thermophilus* and *P. denitrificans* proteins were shipped anaerobically from The Scripps Research Institute to Cambridge on ice.

Characterization of the Overexpressed Bovine Mitochondrial and E. coli 24 kDa Subunits. The *T. thermophilus* (*22*) and *P. denitrificans* (*13*) homologues have been described previously; since the preparations used in this work are comparable, we do not discuss their characterization here. Correct expression of the bovine mitochondrial and *E. coli* proteins was confirmed by N-terminal sequencing (nontagged proteins only) and by measurement of the intact protein mass. For N-terminal sequencing, proteins were separated on an SDS−PAGE gel and then transferred to an Immobilon P membrane (Millipore, Bedford, MA) in a solution of 25 mM tris(hydroxymethyl)aminomethane, 192 mM glycine, and 10% methanol. Excised Coomassie Blue stained bands were analyzed by automated Edman degradation using a Model 494 Procise protein sequencer (Applied Biosystems). Sequences of GAGGALFVHR and MHENQQPQTE were obtained for the bovine and *E. coli* homologues, respectively, identical to those expected. To measure the intact protein mass, samples were applied to a reverse-phase HPLC Aquapore RP-300 column (Perkin-Elmer), eluted with an acetonitrile gradient in 0.1% TFA, and examined using positive ion electrospray mass spectrometry. The Sciex API III^+ triple quadrupole mass spectrometer was tuned and calibrated with a mixture of poly(propylene glycols) over the range of *m*/*z* 59 to 2010 and checked using horse heart myoglobin (average mass 16951.4 Da). Samples were introduced, via a Rheodyne loop, into a stream (3 μL min^{-1}) of 50% aqueous acetonitrile and spectra recorded by scanning the first quadrupole (Q1) from *m*/*z*700 to 1700. Masses of 23812.4 and 18588.2 (standard deviations 1.5 and 1.6) were acquired for the bovine and *E. coli* homologues, respectively, and 25313.4 and 19545.6 (standard deviations 1.1 and 1.6) for the proteins with histidine tags. These are all close to the predicted masses of 23814.4, 18590.1, 25317.0, and 19550.1, confirming the protein sequences; small differences in mass are likely to be due to disulfide bond formation following cluster loss during the HPLC procedure. Finally, protein concentrations were quantified using the BCA protein assay (Pierce), and iron content was measured colorimetrically using 4,7-diphenyl-1,10-phenanthroline (Sigma-Aldrich Ltd.) (*46*).

Characterization of the [2Fe-2S] Clusters in the Bovine Mitochondrial and E. coli Homologues by Electron Paramagnetic Resonance and UV−Visible Spectroscopies. Oxidized and dithionite- (sodium hydrosulfite; Sigma-Aldrich Ltd.) reduced UV−visible spectra were recorded using a UV-1601 Shimadzu spectrometer with the samples sealed in anaerobic quartz SUPRASIL precision cuvettes (Hellma, Southend-on-Sea, U.K.). In each case, spectra were consistent with the presence of a [2Fe-2S] cluster and essentially identical to those previously reported for the *P. denitrificans* (*13*) and *T. thermophilus* (*22*) proteins, though exact peak positions vary slightly. Spectra are shown in Figure 1A.

EPR spectra were recorded on a Bruker EMX X-band spectrometer using an ER 4119HS high-sensitivity cavity maintained at low temperature by an ESR900 continuous flow liquid helium cryostat (Oxford Instruments, Abingdon, U.K.); sample temperature was measured with a calibrated Cernox resistor (Lake Shore Cryotronics Inc.). Power levels were determined to be below microwave saturation, and 100 kHz field modulation amplitudes were chosen to avoid signal distortion and rapid-passage effects. Spectra recorded at 29 K for the bovine mitochondrial and *E. coli* homologues are shown in Figure 1B. The two spectra display very similar *g*-values (though slight differences in line widths are apparent) and correspond closely with those reported previously for the *T. thermophilus* (*22*) and *P. denitrificans* (*13*) homologues; the spectrum of histidine-tagged bovine mitochondrial protein was indistinguishable from that without a histidine tag.

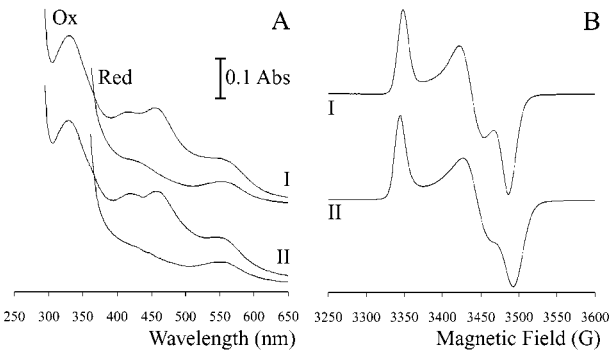

FIGURE 1: Spectroscopic characterization of the [2Fe-2S] clusters of the *E. coli* (I) and bovine mitochondrial (II) 24 kDa homologues. (A) UV−visible spectra of the clusters in the oxidized and sodium dithionite reduced forms. Cluster concentration is approximately 50 μM; clusters were reduced by anaerobic addition of 1 mM sodium dithionite from a concentrated stock solution. Peak absorption maxima in the oxidized form are 330, 416, 455, and 550 for the *E. coli* homologue and 330, 419, 457, and 550 for the bovine mitochondrial homologue. Solution conditions: pH 8.0, 10 mM sodium acetate, MES, HEPES, and TAPS buffers, 0.1 M NaCl, 20 °C. (B) EPR spectra of the reduced clusters. Samples containing between 150 and 250 μM [2Fe-2S] cluster were prepared anaerobically by reduction with a 10-fold excess of sodium dithionite and frozen immediately. EPR conditions: microwave frequency 9.375 GHz, microwave power 2 mW, modulation amplitude 10 G, modulation frequency 100 kHz, time constant 2.65 ms, conversion time 10.24 ms, sample temperature 29 K. $g_{x,y,z}$-values are 1.921, 1.948, and 2.001 for the *E. coli* homologue and 1.917, 1.944, and 2.003 for the bovine mitochondrial protein.

Protein−Film Voltammetry. Reduction potentials for the 24 kDa subunit [2Fe-2S] clusters were measured by protein−film voltammetry. Solution pH values were controlled by a mixture of four buffers chosen from 10 mM sodium acetate, 4-(2-hydroxyethyl)piperazine-1-ethanesulfonic acid (HEPES), 2-morpholinoethanesulfonic acid (MES), *N*-[tris(hydroxymethyl)methyl]-3-aminopropanesulfonic acid (TAPS), and 3-(cyclohexylamino)-1-propanesulfonic acid (CAPS) (total buffer concentration 40 mM), according to pH. Potentials were confirmed to be independent of buffer composition. The pH of each solution was checked immediately following measurement, at the experimental temperature, using a standard glass electrode calibrated at temperature according to known standards (*47*). NaCl, at varying concentrations as specified in the text, was used as supporting electrolyte, and the effects of high Na^+ concentration on pH measurement were corrected by standard formulas (*48*). To prepare the protein film, a protein solution (200 μM, pH 7.5) was applied directly to a fresh pyrolytic graphite edge electrode surface [polished with 1 μm alumina (Buehler, Lake Bluff, IL), sonicated, and rinsed thoroughly with Millipore water] and then placed into solution in an all-glass electrochemical cell fitted with a platinum counter electrode. A standard calomel reference electrode was used, separated from the cell by a Luggin capillary, and all potentials were corrected to the

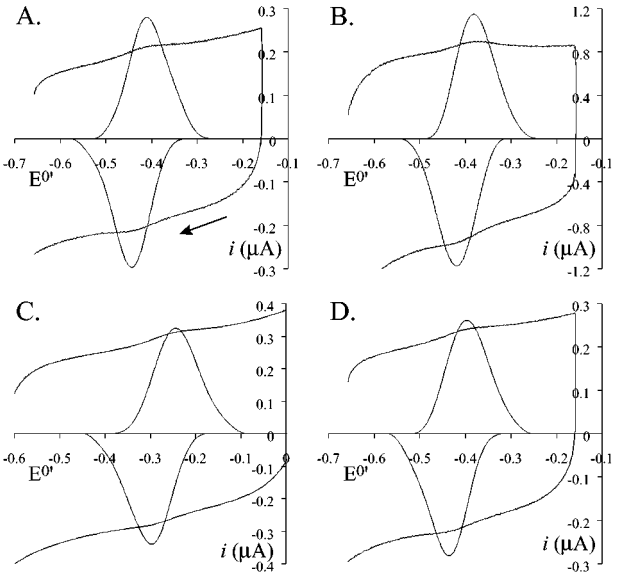

FIGURE 2: Typical film voltammograms showing an example from each of the four different proteins discussed and also the four different conditions: high (2 M NaCl) and low (0.01 M NaCl) ionic strength and high (pH 9) and low (pH 5) pH values. (A) *T. thermophilus* (with histidine tag), pH 9.05, 10 mM NaCl. (B) *P. denitrificans* (with histidine tag), pH 5.28, 2 M NaCl. (C) *E. coli* (with histidine tag), pH 5.05, 10 mM NaCl. (D) bovine mitochondria (without histidine tag), pH 9.05, 2 M NaCl. All data were recorded at 20 °C, scan rate of 20 mV s^{-1}, with solution conditions as described in Experimental Procedures.

standard hydrogen electrode scale (*48*). The cell was encased in a Faraday cage to minimize electrical noise, thermostated using a water jacket, and housed in an anaerobic glovebox (O_2 ~ 1 ppm; Belle Technology). Analog-scan cyclic voltammetry was performed using an PGSTAT30 Autolab electrochemical analyzer (Eco-chemie, Utrecht, The Netherlands) equipped with ADC750 and Scan-Gen modules. Remaining electrical noise was removed by Fourier transformation, provided that signal and noise were on sufficiently separate time scales, and background currents, attributable to electrode capacitance and surface chemistry, were subtracted using an in-house analysis program (courtesy of Dr. H. A. Heering) which fits a cubic spline function to the baseline in regions sufficiently far from the peak and assumes continuation of a similar, smooth function throughout the peak region. Reduction potential (average peak potential) measurements are estimated to be accurate to within ±2 mV.

RESULTS

Reversible [2Fe-2S] Cluster Reduction and Oxidation Observed Voltammetrically. Figure 2 shows film voltammograms for the overexpressed 24 kDa (NQO2, NUOE) subunits of *T. thermophilus*, *P. denitrificans*, *E. coli* and bovine heart mitochondria recorded under a range of different conditions. In each case the scan rate is sufficiently slow that further decrease did not result in any change of the average peak potential, and this value can thus be equated to an equilibrium (Nernstian) reduction potential. The four conditions are chosen to be representative of the range of our experiments: high and low ionic strength and high (pH 9) and low (pH 5) pH values. In all cases the peak separation is small and thus diagnostic of film-bound rather than diffusing protein, typically being 20 mV at high pH (10 mV

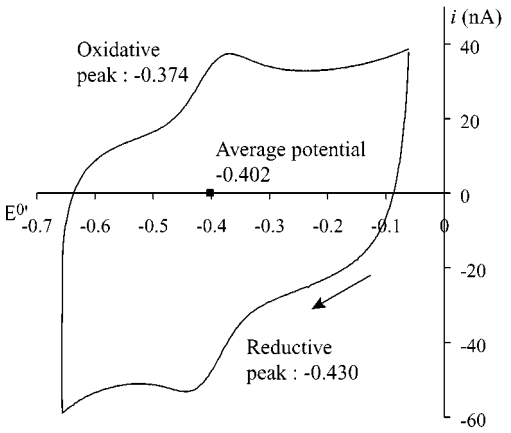

FIGURE 3: Diffusional voltammogram recorded for the *P. denitrificans* [2Fe-2S]-containing homologue (with histidine tag). The protein is free in solution (~150 μM), and electron transfer is controlled by diffusion to the electrode surface, as demonstrated by the large peak separation (56 mV). Conditions: pH 8.0, 1.05 M NaCl, 20 °C, scan rate 1 mV s^{-1}, buffer as described in Experimental Procedures. The average peak potential (−0.402 V) is very close to the potential recorded for the protein adsorbed to the electrode surface under identical conditions (−0.403 V).

s^{-1}) but increasing at lower pH; peak half-height widths are compact (<95 mV at high pH, also slightly increased at low pH), indicating only limited thermodynamic dispersion within the film; peak areas are consistent with formation of a monolayer or submonolayer of protein (coverage ≤ 1.5 × 10^{-11} mol cm^{-2}) on the electrode surface.

Where possible, diffusional voltammetry was used to confirm that film potentials are representative of the potential exhibited by the protein in solution. A typical example is shown in Figure 3. The *T. thermophilus*, *P. denitrificans*, and *E. coli* 24 kDa proteins all produced reversible diffusional voltammograms; however, the native bovine mitochondrial 24 kDa protein, which does not carry an N-terminal histidine tag (see below), did not show any signal. One possible explanation is that the histidine tag promotes a favorable orientation for electron transfer, at the electrode, during transient contact from bulk. Diffusional voltammetry is characterized by larger peak separations (theoretically 58 mV at 20 °C, rather than 0 mV for an adsorbed film) and a linear dependence of peak current upon (scan rate)$^{1/2}$; identifying bulk mass transfer is thus straightforward (*48*). For the solution potential to equal that in the protein−film, the protein can only weakly interact with the surface (no major structural change), and there must be no difference between the free energies of adsorption of the oxidized and reduced forms. Table 1 compares reduction potentials measured by the two methods; various pHs and ionic strengths were evaluated, though at low pH protein instability and insolubility precluded any solution measurement. The close correspondence between solution and film values confirms that adsorption effects are not responsible for the potential variations discussed below. All of our further experiments were therefore carried out using film voltammetry, since this does not necessitate exchanging the protein between different solution conditions, thus facilitating more rapid and reproducible measurements over a wider range of conditions.

Comparison of Systems with and without Histidine Tags. Use of a histidine tag is particularly advantageous for the

Table 1: Comparison of Reduction Potentials Measured with the Protein Diffusing and by Using the Protein−Film Configuration

protein	pH	[NaCl] (M)	*T* (°C)	$E_{diffusion}$	ΔE_{peak} (mV)	$E_{adsorbed}$
T. thermophilus with His tag	7.7	1.00	0	−0.375	75	−0.376
T. thermophilus with His tag	8.0	0.10	0	−0.403	89	−0.400
T. thermophilus H79A	8.0	0.01	0	−0.405	89	−0.411
T. thermophilus	8.0	0.10	0	−0.404	71	−0.400
P. denitrificans with His tag	8.0	1.05	20	−0.402	56	−0.403
E. coli with His tag	9.0	2.00	20	−0.286	146	−0.282

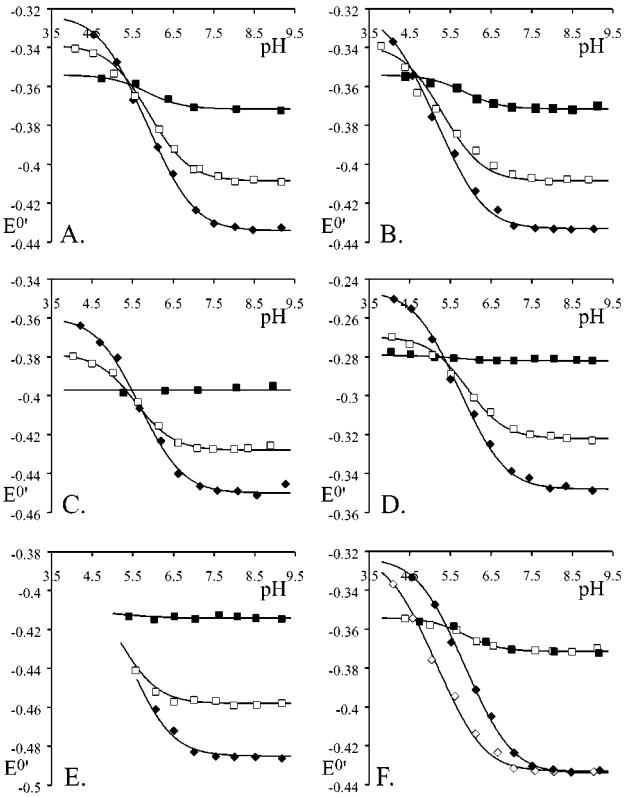

FIGURE 4: Reduction potential vs pH for each of the different species investigated at three different salt concentrations (■, 2 M NaCl; □, 0.1 M NaCl; ◆, 0.01 M NaCl), at 20 °C, with solution conditions as described in Experimental Procedures. (A) *T. thermophilus* protein with histidine tag. (B) *T. thermophilus* protein without histidine tag. (C) *P. denitrificans* protein with histidine tag. (D) *E. coli* protein with histidine tag. (E) Bovine mitochondrial protein without histidine tag. (F) A comparison of the two *T. thermophilus* proteins, with and without histidine tag. Parameters for the data fits are given in Table 2.

overexpressed 24 kDa proteins, since rapid and anaerobic purification minimizes oxidative loss of the iron−sulfur cluster. For the *T. thermophilus*, *P. denitrificans*, and *E. coli* homologues, samples with ∼70%, ∼30%, and ∼70% cluster incorporation, respectively, were produced and gave stable and reproducible voltammetric signals. Direct comparison with native (nontagged) *T. thermophilus* protein showed the effect of the histidine tag on reduction potential to be only slight (see Figure 4 and below), and, thus, although the native protein (cluster incorporation ∼70%) also gave reversible voltammetry over a wide range of conditions, the ease and rapidity of purification led us to adopt the tagged system for our further studies. The *E. coli* homologue was also

Scheme 1: Square Scheme Describing the Coupled Proton−Electron Transfer Process Adopted as Model I

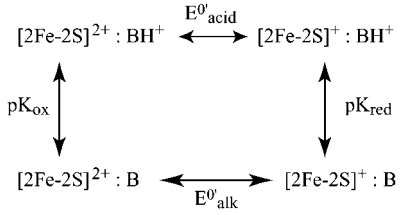

expressed without a histidine tag and purified using a procedure modified from that for the bovine mitochondrial protein. However, the cluster content was considerably decreased, and a significant amount of dimerization was observed, suggesting either cluster loss during purification or incomplete cluster formation during cell growth. Consequently, our best (nontagged) preparations gave only very limited voltammetric results, though potentials were again very close to those of the histidine-tagged equivalent. A very different situation, however, was found for the bovine mitochondrial homologue. In this case, while native protein could be isolated with a cluster content of ∼55% and kept monomeric by the absence of oxygen, the histidine-tagged variant contained significantly less cluster (≤20%), and no voltammetric signals could be observed. Although numerous growth conditions were explored, it was not possible to significantly increase the cluster content of this protein; thus for the mitochondrial homologue we describe only results on the native (nontagged) protein. The lack of signal probably results directly from the low cluster content, perhaps because apoprotein blocks the electrode surface; we note that EPR and UV−visible spectra for the native and tagged preparations are indistinguishable.

Variation of Reduction Potential with pH. In all cases (*T. thermophilus* NQO2, *P. denitrificans* NQO2, *E. coli* NUOE, and bovine heart mitochondria 24 kDa protein) the reduction potential has a similar qualitative pH dependence. At high ionic strength (the upper limit of our experiment is 2 M NaCl) virtually no pH dependence is observed. At high pH, high ionic strength produced a more stable protein film, indicating that protein/electrode-surface interactions contain a hydrophobic contribution or that both protein and surface have a negative charge and require shielding from one another. At low pH, both protein coverage and film stability were decreased, and increasing the salt concentration did not result in any improvement. This alternate behavior is likely to result from the reversal of the protein charge at low pH (see below), and the protonation of graphite surface functionalities at around pH 5.6, causing a decrease in surface negative charge density or perhaps a change in surface polarity (*49*). In all cases, reduction potentials could be measured between pH 5 and pH 9 in 2 M NaCl.

As the ionic strength is decreased, a pH dependence develops. Figure 4 shows the variation of reduction potential with pH, for each protein, at three different concentrations of added NaCl: 10 mM, 0.1 M, and 2 M NaCl. Qualitatively, all of the proteins show remarkably similar behavior, though variations in p*K* and potential values are observed. For each NaCl concentration and each protein, the data can be fitted using the square scheme (Scheme 1) and the equation (eq 1) derived from it (*50*). Equation 1 and Scheme 1 provide four characteristic parameters for each set of data: pK_{ox} and

$$E^{0\prime}_{obs} = E^{0\prime}_{alk} - \frac{RT}{nF}\ln\left[\left(1+\frac{a_{H+}}{K_{ox}}\right)/\left(1+\frac{a_{H+}}{K_{red}}\right)\right] \quad (1)$$

pK_{red} (the apparent pK values of the ionizable group with the cluster oxidized and reduced, respectively) and $E^{0\prime}_{alk}$ and $E^{0\prime}_{acid}$ (the pH-independent reduction potentials achieved at the alkaline and acid limits). Values are presented in Table 2. Figure 4F compares the two forms of the *T. thermophilus* protein (with and without histidine tag) and shows that the histidine tag affects the pK of the ionizable residue but not the pH-independent values, $E^{0\prime}_{alk}$ and $E^{0\prime}_{acid}$, thus shifting the curve slightly in *x*. pK and E values are expected to vary with ionic strength, since increased ionic strength preferentially stabilizes the more highly charged state and also shields interactions between charged groups. For the lowest NaCl concentration shown in Figure 4, 10 mM NaCl, the difference between $E^{0\prime}_{alk}$ and $E^{0\prime}_{acid}$ is approximately 100 mV in all cases. The lower limit of 10 mM NaCl is arbitrary (electrochemical experiments require a supporting electrolyte to maintain solution conductivity), and in fact the difference between $E^{0\prime}_{alk}$ and $E^{0\prime}_{acid}$ (and correspondingly between pK_{ox} and pK_{red}) continues to increase further as the ionic strength is further decreased (see below).

By applying Scheme 1, we are assuming that changes in the reduction potential of the cluster result from changes in the ionization (protonation) state of a single residue. This will be referred to as model I. Since the cluster can sense the electrostatic potential from the ionizable residue, it follows that the residue can also sense the reduction state of the cluster; thus in Scheme 1 pK depends on oxidation state, and E depends on protonation state (*18*, *19*). As ionic strength increases, electrostatic interaction between the two charged sites is gradually screened out, until at the limit of high ionic strength the two sites operate independently and the reduction potential becomes pH-independent. Thus, for the two sites to be *tightly* coupled, as would be required for a physiological redox-coupled proton transfer involved in energy transduction, the environment must be of low dielectric; at present the lack of structural information on complex I precludes an independent evaluation of this situation.

Model I : A Specific Residue Imposes the pH Dependence. Since a pH-dependent reduction potential is suggestive of coupled electron−proton transfer (*18*, *19*) and since little is known about how complex I couples electron and proton transfer, it is imperative to understand the physical reason for the pH-dependent reduction potential of the 24 kDa subunit [2Fe-2S] cluster, also observed in intact complex I by EPR spectroscopy (*10*, *11*, *51*−*53*). Initially, we adopt model I and Scheme 1 as our hypothesis; in this context the key is clearly the identity of the ionizable residue. Figure 5 shows an alignment of our four homologues, the four cysteine ligands forming a solid reference. Several candidate ionizable residues, having the following characteristics, were identified. (i) The residue is aspartate, glutamate, or histidine. Asp or Glu are interchangeable, being both negatively charged and differing only by a side chain $-CH_2-$ group, but positively charged His must be conserved. All Asp, Glu, and His residues are highlighted in Figure 5. (ii) The residue lies inside the protein "core", marked by arrows in Figure 5, and is thus confined to a sequence that is present in all homologues; N- or C-terminal extensions were therefore excluded. (iii) Only residues in the same or adjacent positions were considered, as small structural changes within the same fold may result in adjacent residues being structurally conserved. (iv) Residues forming groups of similarly charged residues, rather than simple and isolated point charges, were considered unlikely candidates since intraresidue interactions would be expected to produce a more complex pH dependence; this excluded from our consideration residues 19−21 and 137−139 (all numbering is for the *T. thermophilus* homologue). Two candidates, His79 and Asp114, circled in Figure 5, were therefore identified. However, since mutants were to be constructed in histidine-tagged *T. thermophilus* protein, due to its ease of purification and good voltammetric signals, two further residues, Glu123 and His129, also circled, were additionally considered, being immediately adjacent to ligating cysteines in this homologue.

Table 2: Reduction Potentials (±5 mV) and pK Values (±0.1) for the 24 kDa Subunit [2Fe-2S] Clusters, as Defined in Scheme 1

	$E^{0\prime}_{alk}$	$E^{0\prime}_{acid}$	ΔE	pK_{ox}	pK_{red}	ΔpK
T. thermophilus (with His tag)						
0.01	−0.434	−0.324	0.110	4.90	6.80	1.90
0.1	−0.409	−0.339	0.070	5.30	6.50	1.20
2	−0.371	−0.354	0.017	5.70	6.0	0.30
T. thermophilus						
0.01	−0.433	−0.323	0.110	4.20	6.10	1.90
0.1	−0.409	−0.339	0.070	4.70	5.90	1.20
2	−0.372	−0.354	0.018	5.70	6.00	0.30
P. denitrificans (with His tag)						
0.01	−0.450	−0.360	0.090	4.90	6.45	1.55
0.1	−0.428	−0.379	0.049	5.15	6.00	0.85
2	−0.397	−0.397	0			0
E. coli (with His tag)						
0.01	−0.348	−0.246	0.102	4.85	6.60	1.75
0.1	−0.322	−0.270	0.052	5.45	6.35	0.90
2	−0.281	−0.279	0.002	5.55	5.60	0.05
bovine mitochondria						
0.01	−0.485				6.20	
0.1	−0.458				5.70	
2	−0.414	−0.414	0			0

Each mutant protein was characterized using protein−film voltammetry as described above. Data are shown in Figure 6, for comparison with Figure 4, and quantified in Table 3. It is obvious that none of the four point mutations affect the pH dependence of the reduction potential; thus the ionizable residue of Scheme 1 has not been identified. While it is possible that different and less conserved residues produce a similar pH dependence in each different case, this dramatically increases the possibilities and was not considered a viable hypothesis. In addition, two further lines of reasoning cast considerable doubt on the applicability of Scheme 1. First, while all data at 20 °C could be fit well using Scheme 1, experiments at 0 °C showed, to varying degree, a systematic error developing in the data fit; such data require two (or more) ionizable residues to produce a reasonable fit, thus effectively resolving the curve into more than one component. The degree to which this effect is manifest varies between homologues and for different point mutations; an example, that of the D114N mutant, is shown in Figure 7. Second, the structure of the homologous *A. aeolicus* ferredoxin (*30*), sequence also aligned in Figure 5, provided an indication of which core residues might be expected to be in the cluster proximity. On first inspection, the cysteine

FIGURE 5: Sequence alignment for the four 24 kDa protein homologues. Sequences were aligned using ClustalW, and minor adjustments made on the basis of secondary structure predictions; a consensus sequence is also presented. Asp, Glu, and His residues are shaded, and the conserved cysteines which ligate the cluster are boxed. Also boxed are the conserved ionizable residues; those with dashed boxes were discarded since they are part of a group of charged residues. Arrows mark the core sequence, present in all homologues, and the specific residues of the *T. thermophilus* protein targeted by mutagenesis are circled. Also shown is an alignment of the ferredoxin from *A. aeolicus* (*30*).

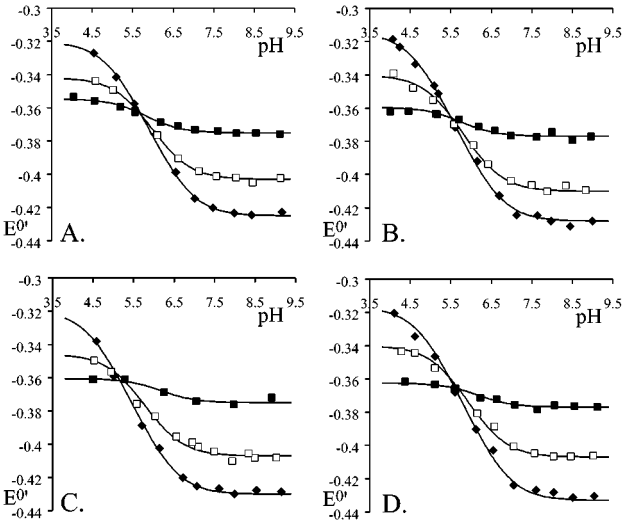

FIGURE 6: Reduction potential vs pH at three different salt concentrations (■, 2 M NaCl; □, 0.1 M NaCl; ◆, 0.01 M NaCl) for each of the mutants (20 °C): (A) H79A; (B) D114N; (C) E123Q; (D) H129A. All of the mutant proteins were forms of the *T. thermophilus* protein with histidine tag. In all cases the behavior was very similar to that of the native protein (Figure 4). Parameters for the data fits are given in Table 3.

Table 3: Reduction Potentials (±5 mV) and p*K* Values (±0.1) for the [2Fe-2S] Clusters in the *T. thermophilus* 24 kDa Subunit Mutants, Compared to the Native Protein, as Defined in Scheme 1

	$E^{0\prime}_{alk}$	$E^{0\prime}_{acid}$	ΔE	pK_{ox}	pK_{red}	ΔpK
T. thermophilus (with His tag)						
0.01	−0.434	−0.324	0.110	4.90	6.80	1.90
0.1	−0.409	−0.339	0.070	5.30	6.50	1.20
2	−0.371	−0.354	0.017	5.70	6.00	0.30
H79A						
0.01	−0.425	−0.320	0.105	5.00	6.80	1.80
0.1	−0.403	−0.342	0.061	5.45	6.50	1.05
2	−0.375	−0.355	0.020	5.65	6.00	0.35
D114N						
0.01	−0.428	−0.315	0.113	4.65	6.60	1.95
0.1	−0.410	−0.340	0.070	5.20	6.40	1.20
2	−0.377	−0.360	0.017	5.60	5.90	0.30
E123Q						
0.01	−0.430	−0.320	0.110	4.50	6.40	1.90
0.1	−0.407	−0.346	0.061	5.25	6.30	1.05
2	−0.375	−0.360	0.015	6.05	6.30	0.25
H129A						
0.01	−0.433	−0.317	0.116	4.80	6.80	2.00
0.1	−0.407	−0.340	0.067	5.35	6.50	1.15
2	−0.377	−0.362	0.015	6.05	6.30	0.25

binding motifs differ due to the position of the first cysteine ligand; however, in the homologous *C. pasteurianum* ferredoxin the position of the second cysteine ligand can be "swapped" into a position closer to that of the complex I 24 kDa subunits (creating a more similar binding motif) while retaining the spectroscopic properties of the native cluster (*32*). In combination with the very similar secondary structure predictions and cluster spectroscopic properties (*31*), this strongly suggests that the 24 kDa proteins share the thioredoxin-type fold of the *A. aeolicus* ferredoxin, with the [2Fe-2S] center located in the disulfide bond position, at the "tip" of the protein (*25*, *30*). However, within the structurally conserved region (from residue 74, *T. thermophilus* numbering) none of the conserved residues identified are predicted to be in reasonable distance of the [2Fe-2S] center. Specifically, His79 (conserved in *A. aeolicus* ferredoxin) lies 16 Å away ([2Fe-2S] Fe1 to His79 Nϵ2), the Cα of Asp114 (estimated by the position of Phe45) approximately 25 Å away (Fe1 to Cα), and the patch of charged residues 137−139 at 16.0 Å (137 Cα to S2), 18.7 Å (138 Cα to S2), and 18.2 Å (139 Cα to S2). For the 24 kDa subunit N-terminal extensions, secondary structure predictions suggest a largely helical conformation; however, this is insufficient information to estimate a cluster distance for the patch of charged residues, positions 19−21. Finally, blast searches (http://www.ebi.ac.uk/blast2/) on the 24 kDa subunit sequences

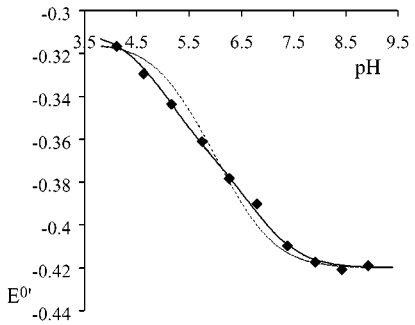

FIGURE 7: Data recorded for the D114N mutant of the *T. thermophilus* protein with 0.01 M NaCl at 0 °C. The two fits to the data are using either one (pK_{ox} = 5.10, pK_{red} = 6.90, $E^{0\prime}_{alk}$ −0.420, dashed line) or two sets of p*K* values (pK_{ox1} = 4.55, pK_{red1} = 5.55, pK_{ox2} = 6.30, pK_{red2} = 7.20, $E^{0\prime}_{alk}$ −0.420, solid line). Thus decreasing the temperature from 20 °C (as shown in Figure 6) to 0 °C results in a change in the variation of reduction potential with pH, which cannot be accounted for by the influence of a single ionizable residue (Scheme 1).

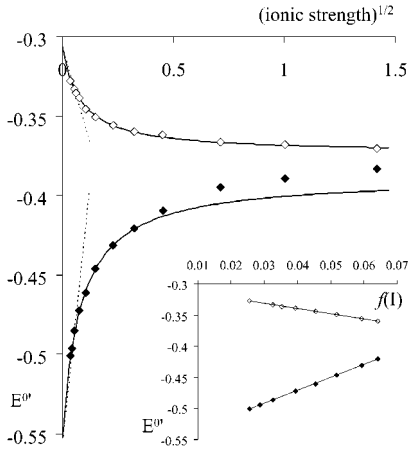

FIGURE 8: Variation of reduction potential with the square root of ionic strength at pH 9 (◆) and pH 5 (◇) for the *T. thermophilus* homologue with histidine tag. Dashed lines indicate the predictions from the Debye−Hückel limiting law and solid lines the fit obtained using extended Debye−Hückel theory. The insert shows the same data plotted using the extended Debye−Hückel theory, with *f*(*I*) plotted against potential; linearity was obtained using aB = 12.5 $M^{-1/2}$. All other parameters are described in the text.

showed that an ionizable residue in positions 19−21, or positions 137−139, is not a well-conserved feature.

Model II: Ionic Strength Dependence. Since targeting specific residues did not provide an explanation for the observed pH dependence, further studies of the histidine-tagged *T. thermophilus* protein were carried out to investigate an alternative physical model for the observed pH and ionic strength (*I*) dependence. Thus, at 20 °C, the dependence of *E* on ionic strength was measured at two pH values (pH 9 and 5), representing the high and low pH limits of our data. Though we controlled the ionic strength of the solution by addition of different concentrations of NaCl, the actual values of ionic strength also take into account the buffer and the NaOH or HCl added to adjust the pH. At pH 9 small concentrations of TAPS buffer were used (either 2 or 10 mM) and at pH 5 small concentrations of acetate. The results are shown in Figure 8, where reduction potential is plotted against square root of *I*. At pH 9, the potential decreases with a decrease in ionic strength, whereas at pH 5 decreasing the ionic strength increases the potential. Qualitatively, these two behaviors can be rationalized as follows: an increase in ionic strength should stabilize the most highly charged state of the protein, relative to the lesser charged state; thus at pH 9 the most highly charged state is the reduced state (reduction potential increases with increased *I*) and at pH 5, the oxidized state (reduction potential decreases with increased *I*). Since reduction of the [2Fe-2S] center adds one negative charge, at pH 9 the protein must have an overall negative charge and at pH 5, an overall positive charge; thus the isopotential point lies between pH 9 and pH 5. In fact, from Figure 4, the isopotential point for each protein may be estimated as the pH at which all three curves intersect (pH 4.5−5.5, though of course the actual isopotential point depends on the cluster oxidation state); these values correspond well to those estimated from the sequences [*T. thermophilus* (with and without histidine tag) 5.85 and 4.75, *P. denitrificans* (with tag) 5.95, *E. coli* (with tag) 5.90, bovine mitochondria 5.50]. We therefore suggest that the apparent redox-coupled proton transfer, observed from the pH dependence recorded at only a *single* ionic strength, is no more than a result of changes in protein charge with pH (our model is simplified by discounting the modulatory effect of electronation upon protonation state). There are thus two key differences with model I. First, changes in charge are due to the protonation and deprotonation of multiple *nonspecific* and *noncoupled* residues, rather than of a single, strongly coupled residue. Second, electronation of the cluster does *not* affect the protonation state of the protein, which is simply a function of pH. Scheme 1 does therefore not apply to model II.

A quantitative understanding of the change in potential with ionic strength (*I*) and pH requires further analysis. In an ionic solution, clustering of counterions around a charged species (the ionic atmosphere) creates a nonrandom distribution of ions, thus altering the free energy of the system and causing the reduction potential to deviate from the value it adopts at zero ionic strength ($E_{I=0}$). The simplest theory with which to model this behavior, Debye−Hückel theory, describes the dependence of the activity coefficient on ionic strength by making a number of key assumptions, which include that ions are to be regarded as point charges and that there is no ion pair formation (specific ion binding) (*54*, *55*). When combined with the Nernst equation, the simplest form of the Debye−Hückel theory, the Debye−Hückel limiting law, leads to the equation:

$$E^{0\prime}_{obs} = E^{0\prime}_{I=0} - (\ln 10)\frac{RT}{nF}(z_{ox}^{\,2} - z_{red}^{\,2})A\sqrt{I} \qquad (2)$$

z_{ox} and z_{red} are the charges on the oxidized and reduced states, respectively, *A* is the Debye−Hückel constant (0.512 $M^{-1/2}$ in water at 25 °C), and *I* is ionic strength (M). Obviously, the difference in the data at high and low pH is embodied, in eq 2, in the values of z_{ox} and z_{red}, which are strongly pH-dependent. Thus, the reduction potential, at given pH, is predicted to depend linearly on the square root of ionic strength. However, Figure 8 shows that this is clearly not the case, though best fits are shown by the dotted lines for the data at the lowest values of *I*, where the Debye−Hückel limiting law is most likely to apply. The Debye−Hückel model can, however, be applied to higher *I* values by the use of extended Debye−Hückel theory, as stated by the

equation:

$$E^{0\prime}_{\text{obs}} = E^{0\prime}_{I=0} - (\ln 10)\frac{RT}{nF}(z_{\text{ox}}^{\ 2} - z_{\text{red}}^{\ 2})A\frac{\sqrt{I}}{1 + aB\sqrt{I}} \quad (3)$$

Theoretically, B is a second constant, 3.291×10^9 m^{-1} M$^{-1/2}$ in water at 25 °C, and a is the closest distance of ionic approach, though aB has come to be generally regarded as an experimental parameter. Data were fitted by plotting potential against $f(I) = I^{1/2}/(1 + aBI^{1/2})$ and by optimizing the parameter aB, to achieve a linear variation (for $I \leq 0.1$ M), as shown in the insert to Figure 8. In this way, the curved lines in Figure 8 were obtained, showing that a good fit is achieved over a wide range of ionic strength, deviating from the experimental data only at the highest I values, at pH 9. Though appearing conclusive at first sight, our fit is however somewhat empirical, as values of z_{ox}, z_{red}, and a are unrestrained by any physical model; values obtained are $z_{\text{ox}} = +15$ (pH 5) and $z_{\text{ox}} = -34$ (pH 9), assuming that the charge decreases by one unit on reduction, and $a = 38$ Å. While all values are of the correct order of magnitude, the charges are too large for a protein of this size at moderate pH, though it is possible that specific ion binding enhances the charge. In reality, it is surprising that this simple theory describes even semiquantitatively the behavior of such a complex entity as a protein molecule, with conformational flexibility, significant size, and the capability of carrying numerous unevenly distributed surface charges—thus directly contradicting a number of assumptions inherent in the derivation of the Debye−Hückel equations (*54*, *55*). In addition, our system is a mixed electrolyte system, since the activity coefficient being evaluated is that of the protein, whereas a simple salt, NaCl, is being used to control the ionic strength. Finally, extended Debye−Hückel theory is not expected to cover the whole range of ionic strength, and further theories such as that of Robinson and Stokes, which emphasizes the solvation of solute ions, are required to deal with yet higher I values (*54*, *55*). With this in mind, however, a number of previous studies, particularly on cytochromes, have successfully used extended Debye−Hückel theory to characterize ionic-strength dependent protein reduction potentials and to investigate the effects of specific anion binding by extrapolation to null ionic strength (*56*−*59*). For the purposes of this publication, we consider it sufficient to have demonstrated that the apparent pH dependence of the reduction potential of the [2Fe-2S] cluster results simply from nonspecific ionization processes occurring as a result of pH changes.

DISCUSSION

Reduction Potentials of the 24 kDa Subunit [2Fe-2S] Clusters. Initially, we consider only the reduction potentials exhibited in high ionic strength, thus comparing the "intrinsic" electron affinities of the four [2Fe-2S] clusters, unaffected by variations resulting from changes in pH. From Figure 4 and Table 2, the *E. coli* [2Fe-2S] cluster displays the highest potential, −0.28 V, followed by *T. thermophilus*, −0.37 V, *P. denitrificans*, −0.40 V, and bovine mitochondrial 24 kDa, −0.41 V; our cluster therefore adopts a potential range of approximately 0.13 V. In the absence of a detailed structure interpretation of these differences, likely to result from variations in solvent accessibility, and the positions and charges of nearby residues, is precluded; thus we discuss only their possible significance. First, the optimal growth temperature of *T. thermophilus* is significantly higher than in the experiment reported in Figure 4. With the histidine-tagged protein we have measured the reduction potential as a function of temperature, up to 70 °C, and observed a decrease in potential to −0.41 V (2 M NaCl, pH 6.5). The *T. thermophilus*, *P. denitrificans*, and bovine clusters are thus very similar in potential (−0.40/−0.41 V), whereas the *E. coli* cluster potential is significantly higher (−0.28 V). This difference may be interpreted in several ways: (i) It does not result from the different enzymes being tuned for electron transfer to different quinones. Bovine mitochondrial complex I and *T. thermophilus* complex I, with very similar cluster potentials, transfer electrons to ubiquinone and menaquinone, respectively, while *E. coli* complex I, with the higher potential, also uses predominantly ubiquinone under aerobic conditions. (ii) *E. coli* complex I has recently been suggested to be a Na^+-translocating enzyme, in contrast to the other enzymes discussed here which are all proton-translocating (*60*). However, while these two features can be superficially correlated, it is not clear why they should be functionally related or interdependent. (iii) Perhaps the most likely explanation is that varying the exact potential of the [2Fe-2S] cluster, within the range reported here, actually has little effect on the *rate* of catalysis by complex I (*61*); the cluster potential has therefore not been constrained by selection and, consequently, adopts a range of values.

Redox-Linked Protonation at the 24 kDa Subunit [2Fe-2S] Cluster? Virtually nothing is currently understood about the mechanism of energy transduction in complex I. Two iron−sulfur clusters, the [2Fe-2S] cluster in the 24 kDa subunit and cluster "N2", the location of which is still questionable, are known to have reduction potentials that vary with pH (*10*, *11*); this is a clear indication of coupled proton−electron transfer (*18*, *19*), and it is therefore imperative to understand the basis of these effects. We have now elucidated the origin of the pH dependence of the 24 kDa subunit [2Fe-2S] cluster potential. Initially, the ionic strength dependence of this behavior was interpreted (model I) to mean that electrostatic interaction between a single ionizable residue and the cluster can be "screened out" by increased ionic strength/dielectric. We now use Scheme 1 to consider how much effect the redox state of the cluster would have upon the protonation state of our ionizable residue, in low ionic strength (10 mM NaCl), should this be the case. By calculating the percentage of the residue protonated, as a function of pH and oxidation state, the maximum change is identified at pH 5.8 (for the histidine-tagged *T. thermophilus* protein), where 80% of the ionizable residue would change its protonation state in response to cluster electronation. Even at this pH therefore, but more generally over the pH range considered, the electron−proton coupling is inefficient and is thus unlikely to play any role in a proton translocation mechanism. Conversely, this is also reflected in the relatively small difference between $E^{0\prime}_{\text{alk}}$ and $E^{0\prime}_{\text{acid}}$ (110 mV), indicating only a limited difference in the free energy of electronation upon protonation. However, we note that the actual dielectric in the vicinity of the cluster in intact complex I is currently unknown; should the local dielectric be low and the access of solvent and solute ions be restricted, the

electrostatic interaction between two spatially remote sites would be propagated, and an "in situ" strong coupling may be produced. For the 24 kDa subunit of complex I, however, we have been unable to identify a specific residue to impose the pH dependence; that the 24 kDa subunit cluster is not involved in proton translocation is consistent with its proposed location, in the membrane extrinsic arm of the complex, probably close to the NADH active site, and thus removed from the transmembrane domains.

Effect of Changes in Protein Charge on Reduction Potential. Our work has shown that the pH dependence of the 24 kDa [2Fe-2S] cluster results from the *ionic strength dependence* of the reduction potential, which is determined by protein charge. Since protein charge is itself pH-dependent (due to the ionization of nonspecific residues), an apparent pH-dependent reduction potential is observed, which is actually the sum of a number of lesser pH dependencies. While these nonspecific, or weakly coupled, protonation events are unlikely to be used in proton pumping, the breakdown of the pH dependence into a number of component parts may actually be exploited by the enzyme. Whereas a single strongly coupled protonation fixes the free energy for the *uncoupled* electron transfer step at the same value over all pHs, a number of smaller pH dependencies allows the enzyme to adopt different free energies for electron transfer at different pHs. This provides a mechanism by which energy conservation may be optimized, as the overall driving force shifts in response to changes in pH (*62*).

More generally, all proteins undergo changes in charge with pH and possess a characteristic isopotential point, and we were therefore led to question why this phenomenon is not more commonly observed in protein voltammetry studies. Since the 24 kDa proteins adsorbed readily to the electrode surface under a wide range of solution conditions, coadsorbates such as neomycin and polymyxin were not employed in our studies. These positively charged organic molecules are commonly used, in conjunction with a graphite electrode, to promote protein adsorption, perhaps via the formation of salt bridges between protein and electrode surface (*36*, *37*). When such coadsorbates were added to our cell solutions, however, large changes in the reduction potential of the 24 kDa subunit clusters were observed, and the pH dependence of the reduction potential (in low ionic strength) was removed. Coadsorbates therefore appear to provide a surface-constrained region of high dielectric, which closely mimics high ionic strength conditions. On one hand, therefore, a coadsorbate may remove an ionic strength dependence which depends on changes in protein charge and result in measured potentials which do not match those observed in solution. On the other hand, in the presence of a coadsorbate it is likely that only strongly coupled ionizations will be observed: this could be regarded as a useful selection for only strongly coupled reactions. Alternatively, as suggested by Bond and co-workers (*63*), strongly charged coadsorbates may bind to the protein, dominating the charge and either preventing, or rendering insignificant, any pH-dependent ionizations; again this would alter the reduction potential and act against a pH dependence being observed. Finally, our results underline the importance of considering the effects of ionic strength upon reduction potential and of not interpreting, at face value, a pH-dependent reduction potential as a definitive sign of a proton-coupled redox process.

Comparison of the Isolated 24 kDa Subunit with Intact Complex I and the Fp Subcomplex. We now compare our results with data from potentiometric (EPR) studies on intact complex I and on the Fp subcomplex of bovine mitochondrial complex I, containing only the 51, 24, and 10 kDa subunits. It is becoming generally accepted that the [2Fe-2S] cluster in the 24 kDa subunit is cluster "N-1a", rather than "N-1b" (named according to the EPR signal) (*10*, *11*). Unfortunately, little can be learned by direct comparison of the EPR signals from the overexpressed 24 kDa subunit with those from complex I, since neither the *g*-values reported for cluster N-1a or cluster N-1b match those of the overexpressed protein (*10*, *11*, *51*−*53*). However, EPR studies on the Fp subcomplex (*64*, *65*) (while varying according to the preparation) have reported spectra which do match closely with those presented here (*66*). It is likely that, since the cluster is exposed on the tip of the protein fold, the spectroscopic characteristics are modified upon removal of the subunit from the complex I interior (where the cluster is likely to physically contact another subunit and to be in the proximity of other redox sites) and its subsequent contact with solvent.

Our voltammetric studies are consistent with the 24 kDa subunit containing cluster N-1a, since EPR studies have suggested cluster N-1a to be pH-dependent, whereas cluster N-1b is not, and since our [2Fe-2S] potentials closely match those measured by EPR for cluster N-1a (*10*, *11*). For bovine mitochondrial complex I, Ingledew and Ohnishi (*51*) reported one pH-independent reduction potential of −240 mV for cluster N-1b and a pH-dependent potential for N-1a, ranging from −320 at pH 6.2 to −480 mV at pH 8.8, with a slope of 1 $H^+/1e^-$ (60 mV per pH unit); data were recorded in 50 mM buffer, which approximates to the low salt (10 mM NaCl) condition described here. However, a significant amount of scatter exists in published measurements of the reduction potential of the 24 kDa subunit [2Fe-2S] cluster (or cluster N-1a). On the basis of the wide range of conditions our experiments have been able to access, we now suggest this may be due to small variations in pH and ionic strength, resulting in surprisingly large variations in potential. In addition, Ohnishi has suggested that confusion has arisen from the low potential of cluster N-1a, which decreases further upon solubilization away from the membrane environment (*10*, *11*) and which has resulted in it remaining EPR silent in a number of cases. An additional anomaly arises for the *P. denitrificans* enzyme. While our data show that the properties of the clusters in all of the homologues are fundamentally similar, EPR data have suggested that the potential of the N-1a cluster in *P. denitrificans* is elevated to −150 mV at pH 7, significantly higher than the other homologous clusters, though, in contrast to N-1b at −270 mV, it retains a limited pH dependence (*52*). At present we have no satisfactory explanation for this discrepancy but note that the anomalous behavior of the *P. denitrificans* 24 kDa cluster has been suggested to be the cause of differences in activity with the bovine homologue, when compared using various assay systems (*67*).

The potential of the 24 kDa subunit [2Fe-2S] cluster is also likely to be affected, to some extent, by whether the subunit is isolated or part of the intact complex, particularly since it is proposed that the [2Fe-2S] cluster is exposed at the tip of a thioredoxin-like fold (*30*). In the absence of structural data for either the 24 kDa subunit or intact complex

I it is difficult to infer how much the cluster environment in the isolated subunit reflects that in the intact complex; this will depend on how much the cluster is protected from solvent by other subunits, the presence of internal water molecules or ions, and also the nature of the surrounding protein matrix. In addition, complex I is an integral membrane protein, and thus even this hydrophilic subunit may be affected by the membrane environment. Comparing the potentials exhibited by the cluster in intact complex I (from EPR spectroscopy) and in the isolated subunit (from voltammetry) provides some insight. Between pH 6 and pH 9 mitochondrial complex I cluster N-1a has a reduction potential which varies with pH by 60 mV/decade (*51*); this places the cluster firmly into a region of low dielectric in the intact complex, on the basis of comparison with the voltammetric data. More fundamentally, we have found that the charge on the isolated subunit (along with the dielectric environment) determines the reduction potential. How this is to be considered when the subunit is integrated into complex I is not clear; it may be that the reduction potential of the [2Fe-2S] cluster will now reflect the charge of the complete complex or, more likely, that the local electrostatic environment, from the 24 kDa subunit and other nearby subunits, will dictate the redox properties of the cluster. Further work is clearly required to determine how the surrounding protein matrix modulates the properties of the cluster, as quantified here, and, furthermore, how similar effects may, or may not, influence the properties of the other redox centers in complex I. Conversely, it is also possible that changes in the charge of the 24 kDa subunit may mediate changes in the conformation of complex I, around the active site, as a result of variations in ionic strength or pH affecting the rate of catalysis.

Role of the 24 kDa [2Fe-2S] Cluster in Complex I Catalysis. The [2Fe-2S] cluster in the 24 kDa subunit in complex I adopts a wide range of potential, from −0.49 to −0.25 V, depending on the species and conditions of pH and ionic strength. First, and most simply, we compare these potentials with those of the other redox couples involved in complex I catalysis. The two-electron potentials of NADH [−0.32 V, pH 7.0 (*50*)] and the active site FMN [−0.38 V, pH 7.5 (*68*)] are close enough that, to a first approximation, the cluster could be expected to exchange electrons reversibly with the active site. The potential of (ubi)quinone is, however, significantly *higher* than that of NADH, and so the 24 kDa subunit [2Fe-2S] potentials (except for the *E. coli* 24 kDa cluster) do not lie between the redox donor and acceptor potentials. Currently accepted potentials for the other complex I iron−sulfur clusters comprise the so-called "isopotential pool" (*10*, *11*) and do lie comfortably between the donor and acceptor potentials. An out-of-line potential is however not unusual in biology and, as discussed by Dutton and co-workers, does not necessarily present a significant kinetic barrier to catalysis (*61*). Furthermore, as pointed out by Hille and Anderson for xanthine oxidase (*69*), this out-of-line potential may be crucial in controlling the transfer of reducing equivalents from the FMN active site to the iron−sulfur clusters in complex I. Including a low potential acceptor (the [2Fe-2S] center) at the start of the iron−sulfur acceptor chain means that the FMN active site is deterred from donating a *single* electron to form the high-energy semireduced state. This is due to the unfavorable thermodynamics for single electron transfer from the FMN [$E_{2/1}$ is estimated as −0.34 V, pH 7.5, in bovine mitochondrial complex I (*68*)] to the low-potential [2Fe-2S] center (−0.48 V, 10 mM NaCl; see Figure 4). However, the lower *average* potential for the two-electron oxidation of FMN [−0.375 V, pH 7.5 (*68*)], in conjunction with the higher *average* potential, −0.365 V, of the first two iron−sulfur centers [most likely the low-potential 24 kDa cluster (−0.48 V) and the [4Fe-4S] cluster in the 51 kDa subunit, N-3 (−0.25 V (*51*)], means that donation of *two* electrons into the chain is much more thermodynamically favorable. Thus the 24 kDa subunit [2Fe-2S] center, known to be one of the iron−sulfur clusters closest to the FMN may, by its low potential, actually aid in preventing formation of an FMN radical intermediate, thus decreasing the likelihood of nonspecific radical formation and oxidative damage.

Conclusion. We have shown that the [2Fe-2S] cluster in the complex I 24 kDa subunit has a potential which varies between −0.28 and −0.42 V (depending on the species) and that this cluster displays a pH-dependent reduction potential, as a result of nonspecific protonations which alter the protein charge as a function of pH. Though the pH dependence, also exhibited by this cluster in intact complex I, is unlikely to be physiologically relevant for coupled proton−electron transfer (proton pumping), the low potential of the cluster may be important in controlling transfer of electrons between the active site and the other iron−sulfur clusters and in minimizing free radical formation. It is now intended to extend this methodology to investigate the other redox components of complex I and to thus create voltammetric "fingerprints" for each of the redox centers, which will in turn form an integral part of studies on the ensemble of centers in the intact enzyme. Though it is not clear to what degree an intact enzyme may be considered the linear result of its individual components, it is hoped that characterizing these components in detail will aid in the construction of a complete mechanistic model for proton-coupled electron transfer in complex I.

ACKNOWLEDGMENT

We thank Dr. Ian M. Fearnley for carrying out mass spectrometry measurements and Drs. John E. Walker and Paula E. Wilks for providing the initial expression plasmid for the bovine mitochondrial 24 kDa protein.

REFERENCES

1. Saraste, M. (1999) Oxidative phosphorylation at the *fin de siècle*, *Science 283*, 1488−1493.
2. Schultz, B. E., and Chan, S. I. (2001) Structures and proton-pumping strategies of mitochondrial respiratory enzymes, *Annu. Rev. Biophys. Biomol. Struct. 30*, 23−65.
3. Walker, J. E. (1992) The NADH:ubiquinone oxidoreductase (complex I) of respiratory chains, *Q. Rev. Biophys. 25*, 253−324.
4. Weiss, H., Friedrich, T., Hofhaus, G., and Preis D. (1991) The respiratory-chain NADH dehydrogenase (complex I) of mitochondria, *Eur. J. Biochem. 197*, 563−576.
5. Grigorieff, N. (1999) Structure of the respiratory NADH:ubiquinone oxidoreductase (complex I), *Curr. Opin. Struct. Biol. 9*, 476−483.
6. Fearnley, I. M., Carroll, J., Shannon, R. J., Runswick, M. J., Walker, J. E., and Hirst, J. (2001) GRIM-19, a cell death regulatory gene product, is a subunit of bovine mitochondrial NADH: ubiquinone oxidoreductase (complex I), *J. Biol. Chem. 276*, 38345−38348.

7. Chomyn, A., Mariottini, P., Cleeter, M. W. J., Ragan, C. I., Matsuno-Yagi, A., Hatefi, Y., Doolittle, R. F., and Attardi, G. (1985) Six unidentified reading frames of human mitochondrial DNA encode components of the respiratory-chain NADH dehydrogenase, *Nature 314*, 592−597.
8. Yagi, T. (1993) The bacterial energy-transducing NADH-quinone oxidoreductases, *Biochim. Biophys. Acta 1141*, 1−17.
9. Yagi, T., Yano, T., Di Bernardo, S., and Matsuno-Yagi, A. (1998) Procaryotic complex I (NDH-1), an overview, *Biochim. Biophys. Acta 1364*, 125−133.
10. Sled, V. D., Friedrich, T., Leif, H., Weiss, H., Meinhardt, S. W., Fukumori, Y., Calhoun, M. W., Gennis, R. B., and Ohnishi, T. (1993) Bacterial NADH-quinone oxidoreductases: Iron−sulfur clusters and related problems, *J. Bioenerg. Biomembr. 25*, 347−356.
11. Ohnishi, T. (1998) Iron−sulfur clusters/semiquinones in complex I, *Biochim. Biophys. Acta 1364*, 186−206.
12. Yano, T., and Yagi, T. (1999) H^+-translocating NADH-quinone oxidoreductase (NDH-1) of *Paracoccus denitrificans*, *J. Biol. Chem. 274*, 28606−28611.
13. Yano, T., Sled, V. D., Ohnishi, T., and Yagi, T. (1994) Expression of the 25-kilodalton iron−sulfur subunit of the energy-transducing NADH-ubiquinone oxidoreductase of *Paracoccus denitrificans*, *Biochemistry 33*, 494−499.
14. Yano, T., Sled, V. D., Ohnishi, T., and Yagi, T. (1996) Expression and characterization of the flavoprotein subcomplex composed of 50-kDa (NQO1) and 25-kDa (NQO2) subunits of the proton-translocating NADH-quinone oxidoreductase of *Paracoccus denitrificans*, *J. Biol. Chem. 271*, 5907−5913.
15. Yano, T., Yagi, T., Sled, V. D., and Ohnishi, T. (1995) Expression and characterization of the 66-kilodalton (NQO3) iron−sulfur subunit of the proton-translocating NADH-quinone oxidoreductase of *Paracoccus denitrificans*, *J. Biol. Chem. 270*, 18264−18270.
16. Yano, T., Magnitsky, S., Sled, V. D., Ohnishi, T., and Yagi, T. (1999) Characterization of the putative 2 x [4Fe-4S]-binding NQO9 subunit of the proton-translocating NADH-quinone oxidoreductase (NDH-1) of *Paracoccus denitrificans*, *J. Biol. Chem. 274*, 28598−28605.
17. Nakamaru-Ogiso, E., Yano, T., Ohnishi, T., and Yagi, T. (2002) Characterization of the iron−sulfur cluster coordinated by a cysteine cluster motif ($CXXCXXXCX_{27}C$) in the Nqo3 subunit in the proton-translocating NADH:quinone oxidoreductase (NDH-1) of *Thermus thermophilus* HB-8, *J. Biol. Chem. 277*, 1680−1688.
18. Hirst, J., Duff, J. L. C., Jameson, G. N. L., Kemper, M. A., Burgess, B. K., and Armstrong, F. A. (1998) Kinetics and mechanism of redox-coupled, long-range proton transfer in an iron−sulfur protein. Investigation by fast-scan protein-film voltammetry, *J. Am. Chem. Soc. 120*, 7085−7094.
19. Chen, K., Hirst, J., Camba, R., Bonagura, C. A., Stout, C. D., Burgess, B. K., and Armstrong, F. A. (2000) Atomically defined mechanism for proton transfer to a buried redox centre in a protein, *Nature 405*, 814−817.
20. Pilkington, S. J., and Walker, J. E. (1989) Mitochondrial NADH-ubiquinone reductase: complementary DNA sequences of import precursors of the bovine and human 24-kDa subunit, *Biochemistry 28*, 3257−3264.
21. Xu, X., Matsuno-Yagi, A., and Yagi, T. (1991) Characterization of the 25-kilodalton subunit of the energy-transducing NADH-ubiquinone oxidoreductase of *Paracoccus denitrificans*: sequence similarity to the 24-kilodalton subunit of the flavoprotein fraction of mammalian complex I, *Biochemistry 30*, 8678−8684.
22. Yano, T., Chu, S. S., Sled, V. D., Ohnishi, T., and Yagi, T. (1997) The proton-translocating NADH-quinone oxidoreductase (NDH-1) of thermophilic bacterium *Thermus thermophilus* HB-8, *J. Biol. Chem. 272*, 4201−4211.
23. Weidner, U., Geier, S., Ptock, A., Friedrich, T., Leif, H., and Weiss, H. (1993) The gene locus of the proton translocating NADH: ubiquinone oxidoreductase in *Escherichia coli*, *J. Mol. Biol. 233*, 109−122.
24. Yano, T., Sled, V. D., Ohnishi, T., and Yagi, T. (1994) Identification of amino acid residues associated with the [2Fe-2S] cluster of the 25 kDa (NQO2) subunit of the proton-translocating NADH-quinone oxidoreductase of *Paracoccus denitrificans*, *FEBS Lett. 354*, 160−164.
25. Meyer, J. (2001) Ferredoxins of the third kind, *FEBS Lett. 509*, 1−5.
26. Johnson, M. K. (1994) Iron−sulfur proteins, in *Encyclopedia of Inorganic Chemistry* (King, R. B., Ed.) pp 1896−1915, Wiley, Chichester.
27. De Luca, G., Asso, M., Bélaïch, J.-M., and Dermoun, Z. (1998) Purification and characterization of the HndA subunit of NADP-reducing hydrogenase from *Desulfovibrio fructosovorans* overproduced in *Escherichia coli*, *Biochemistry 37*, 2660−2665.
28. Verhagen, M. F. J. M., O'Rourke, T. W., Menon, A. L., and Adams, M. W. W. (2001) Heterologous expression and properties of the γ-subunit of the Fe-only hydrogenase from *Thermotoga maritima*, *Biochim. Biophys. Acta 1505*, 209−219.
29. Chatelet, C., and Meyer, J. (1999) The [2Fe-2S] protein I (Shetna protein I) from *Azotobacter vinelandii* is homologous to the [2Fe-2S] ferredoxin from *Clostridium pasteurianum*, *J. Biol. Inorg. Chem. 4*, 311−317.
30. Yeh, A. P., Chatelet, C., Soltis, S. M., Kuhn, P., Meyer, J. and Rees, D. C. (2000) Structure of a thioredoxin-like [2Fe-2S] ferredoxin from *Aquifex aeolicus*, *J. Mol. Biol. 300*, 587−595.
31. Crouse, B. R., Yano, T., Finnegan, M. G., Yagi, T., and Johnson, M. K. (1994) Properties of the iron−sulfur center in the 25-kilodalton subunit of the proton-translocating NADH-quinone oxidoreductase of *Paracoccus denitrificans*, *J. Biol. Chem. 269*, 21030−21036.
32. Golinelli, M.-P., Akin, L. A., Crouse, B. R., Johnson, M. K., and Meyer, J. (1996) Cysteine ligand swapping on a deletable loop of the [2Fe-2S] ferredoxin from *Clostridium pasteurianum*, *Biochemistry 35*, 8995−9002.
33. Galante, Y. M., and Hatefi, Y. (1979) Purification and molecular and enzymic properties of mitochondrial NADH dehydrogenase, *Arch. Biochem. Biophys. 192*, 559−568.
34. Braun, M., Bungert, S., and Friedrich, T. (1998) Characterization of the overproduced NADH dehydrogenase fragment of the NADH:ubiquinone oxidoreductase (complex I) from *Escherichia coli*, *Biochemistry 37*, 1861−1867.
35. Pilkington, S. J., Skehel, J. M., Gennis, R. B., and Walker, J. E. (1991) Relationship between mitochondrial NADH-ubiquinone reductase and a bacterial NAD-reducing hydrogenase, *Biochemistry 30*, 2166−2175.
36. Armstrong, F. A. (1997) Evaluations of reduction potential data in relation to coupling, kinetics and function, *J. Biol. Inorg. Chem. 2*, 139−142.
37. Armstrong, F. A., Heering, H. A., and Hirst, J. (1997) Reactions of complex metalloproteins studied by protein-film voltammetry, *Chem. Soc. Rev. 26*, 169−179.
38. Hirst, J., Sucheta, A., Ackrell, B. A. C., and Armstrong, F. A. (1996) Electrocatalytic voltammetry of succinate dehydrogenase: direct quantification of the catalytic properties of a complex electron-transport enzyme, *J. Am. Chem. Soc. 118*, 5031−5038.
39. Turner, K. L., Doherty, M. K., Heering, H. A., Armstrong, F. A., Reid, G. A., and Chapman, S. K. (1999) Redox properties of flavocytochrome c_3 from *Shewanella frigidimarina* NCIMB400, *Biochemistry 38*, 3302−3309.
40. Pershad, H. R., Duff, J. L. C., Heering, H. A., Duin, E. C., Albracht, S. P. J., and Armstrong, F. A. (1999) Catalytic electron transport in *Chromatium vinosum* [NiFe]-hydrogenase: application of voltammetry in detecting redox-active centers and establishing that hydrogen oxidation is very fast even at potentials close to the reversible H^+/H_2 value, *Biochemistry 38*, 8992−8999.
41. Camba, R., and Armstrong, F. A. (2000) Investigations of the oxidative disassembly of Fe−S clusters in *Clostridium pasteurianum* 8Fe ferredoxin using pulsed-protein-film voltammetry, *Biochemistry 39*, 10587−10598.
42. Way, M., Pope, B., Gooch, J., Hawkins, M., and Weeds, A. G. (1990) Identification of a region in segment 1 of gelsolin critical for actin binding, *EMBO J. 9*, 4103−4109.
43. Miroux, B., and Walker, J. E. (1996) Over-production of proteins in *Escherichia coli*: mutant hosts that allow synthesis of some membrane proteins and globular proteins at high levels, *J. Mol. Biol. 260*, 289−298.
44. Xu, X., Matsuno-Yagi, A., and Yagi, T. (1991) The NADH-binding subunit of the energy-transducing NADH-ubiquinone oxidoreductase of *Paracoccus denitrificans*: gene cloning and deduced primary structure, *Biochemistry 30*, 6422−6428.
45. Wilks, P. E. (1994) Ph.D. Thesis, Cambridge University.
46. Doeg, K. A., and Ziegler, D. M. (1962) Simplified methods for the estimation of iron in mitochondria and submitochondrial fractions, *Arch. Biochem. Biophys. 97*, 37−40.
47. Lide, D. R. (2000) in *Handbook of Chemistry and Physics*, 81st ed., CRC Press, Boca Raton, FL.

48. Bard, A. J., and Faulkner, L. R. (2001) in *Electrochemical Methods*, 2nd ed., Wiley, New York.
49. Armstrong, F. A., Cox, P. A., Hill, H. A. O., Lowe, V. J., and Oliver, B. N. (1987) Metal ions and complexes as modulators of protein-interfacial electron transport at graphite electrodes, *J. Electroanal. Chem. 217*, 331−366.
50. Clark, W. M. (1960) in *Oxidation−reduction potentials of organic systems*, Williams and Wilkins, Baltimore, MD.
51. Ingledew, W. J., and Ohnishi, T. (1980) An analysis of some thermodynamic properties of iron-sulphur centres in site I of mitochondria, *Biochem. J. 186*, 111−117.
52. Meinhardt, S. W., Kula, T., Yagi, T., Lillich, T., and Ohnishi, T. (1987) EPR characterization of the iron−sulfur clusters in the NADH:ubiquinone oxidoreductase segment of the respiratory chain in *Paracoccus denitrificans*, *J. Biol. Chem. 262*, 9147−9153.
53. Meinhardt, S. W., Wang, D.-C., Hon-nami, K., Yagi, T., Oshima, T., and Ohnishi, T. (1990) Studies on the NADH-menaquinone oxidoreductase segment of the respiratory chain in *Thermus thermophilus* HB-8, *J. Biol. Chem. 265*, 1360−1368.
54. Robbins, J. (1972) in *Ions in solution: an introduction to electrochemistry*, Clarendon Press, Oxford.
55. Compton, R. G., and Sanders, G. H. W. (1998) in *Electrode potentials*, Oxford University Press, Oxford.
56. Margalit, R., and Schejter, A. (1973) Cytochrome *c*: a thermodynamic study of the relationships among oxidation state, ion-binding and structural parameters, *Eur. J. Biochem. 32*, 492−499.
57. Gopal, D., Wilson, G. S., Earl, R. A., and Cusanovich, M. A. (1988) Cytochrome *c*: ion binding and redox properties, *J. Biol. Chem. 263*, 11652−11656.
58. Battistuzzi, G., Borsari, M., Dallari, D., Lancellotti, I., and Sola, M. (1996) Anion binding to mitochondrial cytochromes *c* studied through electrochemistry, *Eur. J. Biochem. 241*, 208−214.
59. Battistuzzi, G., Borsari, M., Loschi, L., and Sola, M. (1997) Redox thermodynamics, acid−base equilibria and salt-induced effects for the cucumber basic protein. General implications for blue-copper proteins, *J. Biol. Inorg. Chem. 2*, 350−359.
60. Steuber, J. (2001) The Na^+-translocating NADH:quinone oxidoreductase (NDH1) from *Klebsiella pneumoniae* and *Escherichia coli*: implications for the mechanism of redox-driven cation translocation by complex I, *J. Bioenerg. Biomembr. 33*, 179−186.
61. Page, C. C., Moser, C. C., Chen, X., and Dutton, P. L. (1999) Natural engineering principles of electron tunneling in biological oxidation−reduction, *Nature 402*, 47−52.
62. Rappaport, F., and Lavergne, J. (2001) Coupling of electron and proton transfer in the photosynthetic water oxidase, *Biochim. Biophys. Acta 1503*, 246−259.
63. Xiao, Z., Lavery, M. J., Bond, A. M., and Wedd, A. G. (1999) The dependence of reversible potentials on the form of modification of edge plane pyrolytic graphite electrodes in voltammetric studies on rubredoxin and ferredoxin from *Clostridium pasteurianum*, *Electrochem. Commun. 1*, 309−314.
64. Ohnishi, T., Blum, H., Galante, Y. M., and Hatefi, Y. (1981) Iron−sulfur N-1 clusters studied in NADH-ubiquinone oxidoreductase and in soluble NADH dehydrogenase, *J. Biol. Chem. 256*, 9216−9220.
65. Ohnishi, T., Ragan, C. I., and Hatefi, Y. (1985) EPR studies of iron−sulfur clusters in isolated subunits and subfractions of NADH-ubiquinone oxidoreductase, *J. Biol. Chem. 260*, 2782−2788.
66. Ragan, C. I., Galante, Y. M., Hatefi, Y., and Ohnishi, T. (1982) Resolution of mitochondrial NADH dehydrogenase and isolation of two iron−sulfur proteins, *Biochemistry 21*, 590−594.
67. Zickermann, V., Kurki, S., Kervinen, M., Hassinen, I., and Finel, M. (2000) The NADH oxidation domain of complex I: do bacterial and mitochondrial enzymes catalyze ferricyanide reduction similarly? *Biochim. Biophys. Acta 1459*, 61−68.
68. Sled, V. D., Rudnitzky, N. I., Hatefi, Y., and Ohnishi, T. (1994) Thermodynamic analysis of flavin in mitochondrial NADH: ubiquinone oxidoreductase (complex I), *Biochemistry 33*, 10069−10075.
69. Hille, R., and Anderson, R. F. (2001) Coupled electron/proton transfer in complex flavoproteins, *J. Biol. Chem. 276*, 31193−31201.

BI026026F